

Bidensity Particle Laden Flows on an Incline

Jessica Bojorquez, Josh Crasto, Dominic Diaz, Margaret Koulikova,
Tameez Latib, Aviva Prins, Andrew Shapiro, and Clover Ye

Math199, Spring 2017

PI: Andrea Bertozzi

Advisors: David Arnold, Claudia Falcon, Michael Lindstrom

Abstract

Particle laden slurries are ubiquitous in nature and in industrial settings, whenever particles are suspended or transported in a solvent. However, polydisperse thin film particle laden flow is poorly understood, necessitating the development of a comprehensive quantitative model. Previous research on gravity driven bidensity viscous thin film flows exclusively studied a constant volume. We present an analysis on the behavior of these flows due to two conditions: constant volume and continuous pouring of slurry, i.e. constant flux. We classified flows along a straight track as 'settled' or 'ridged' for different inclination angle α and particle concentration ϕ . Low values of α and ϕ are correlated with the settled regime, and high values with the ridged regime. We observed interesting fingering phenomena in the constant flux case, which requires further investigation. Additionally, studying different particle sizes will give us a more complete understanding of the dynamics.

Contents

1	Introduction	4
2	Theory	4
3	Experimental Procedure	11
3.1	Materials and Apparatus	11
3.1.1	Materials	11
3.1.2	Track	12
3.1.3	Laser	13
3.1.4	Camera	13
3.1.5	Pump	13
3.2	Procedure	13
3.2.1	Preparation of PDMS and Particle Mixture	14
3.2.2	Track Setup	14
3.2.3	Measurement of Flow Rate	14
3.2.4	Front Tracking for Constant Volume	15
3.2.5	Front Tracking for Constant Flux	15
3.2.6	Height Profile Experiments	16
4	Data Analysis	16
4.1	Front Tracking	17
4.2	Height Profile	19
4.3	Error	20
4.3.1	Front Tracking	20
4.3.2	Height Profile	22
5	Results	22
5.1	Constant Volume	23
5.1.1	Front Tracking	23
5.2	Constant Flux	26

5.2.1	Front Tracking	26
5.3	Height Profile	29
6	Experimental Error	30
7	Conclusion	30
8	Acknowledgements	31
References		32

1 Introduction

Particle laden slurries are pervasive in many contexts, including environmental, industrial, and biological fields. In particular, the suspension and segregation of particles in a shear flow are relevant to the study of landslides, oil spills, and wastewater treatment [1, 2, 3]. The design of helical spiral separators in mining processes and other industrial uses of shear induced particle migration lack quantitative models. At the end of their paper, Lee et al. state that a greater understanding of polydisperse slurries is necessary to understand the behavior of particles in spiral separators [4]. The first step towards studying a sophisticated helical geometry is to develop a strong model for a simpler scenario.

We studied the characteristics of particle laden slurries on a straight track with adjustable angle. The mixture flowed down the incline due to gravity, a constant force. We investigated two initial configurations at the top of the track: constant volume and constant flux. In the constant volume case, we added a fixed quantity of the mixture. In the constant flux case, we used a pump to continuously deposit the slurry. Both cases are considered to be a type of Stokes flow.

The Stokes flow occurs at a small Reynolds number ($Re = uL/\nu \ll 1$). The presence of particles in the mixture increased the effective dynamic viscosity ν relative to the velocity u and length L . The resulting non turbulent flow caused the particles to be suspended over a longer time scale over the course of the experiment. The particles, hindered by the viscosity of the mixture, experienced shear force.

Unlike gravity, shear force is not evenly distributed along the track. The open surfaces at the top and front of the slurry have no shear stress. Thus, the particles experienced shear-induced migration, i.e. they moved from high concentration to low concentration [5]. In contrast, gravity induced migration caused the particles to move down and towards the bottom of the track. The competing forces cause two types of regimes: ridged and settled. In the ridged regime, the shear forces are dominant, causing particles to be suspended and pushed towards the front of the flow. In the settled regime, the gravitational force is dominant, causing the particles to sink [6, 7]. Previous research has classified these regimes for bidensity particle laden flows with constant volume initial conditions [8, 9].

2 Theory

We consider the flow of a viscous, incompressible, clear fluid down a slope in the Stokes regime (Reynolds number $Re = uL/\nu \ll 1$, with u = speed of the fluid, L = length of track, and ν the kinematic viscosity). Thus our governing equations are the incompressible Navier-Stokes equations as follows:

$$\nabla \cdot \vec{u} = 0 \quad (1)$$

$$\vec{u}_t - \nu \Delta \vec{u} + \frac{\nabla P}{\rho} = \vec{g} \quad (2)$$

Since the Reynolds number is small, we are in the Stokes regime. By careful choice of nondimensionalized variables, we find $u_t = 0$.

Where \vec{u} is the velocity, P is the pressure, \vec{g} is the acceleration due to gravity, ρ is the density of the fluid, and ν is the kinematic viscosity. We can assume that ρ is constant throughout the fluid because we are assuming that the fluid is incompressible. Note that \vec{u} and P are all measured within a sphere of radius δ around a single point so they are the local velocity and pressure of the fluid.

We also assume that the incline is wide enough that we can assume no y -dependence of the flow, and that the height scale of the fluid H is much smaller than the length scale of the track L .

We define our coordinate system in Figure 1:

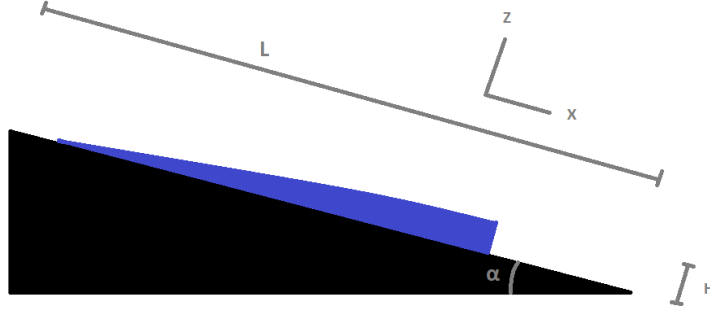


Figure 1

Let $\vec{u} = (u, w)$ where u is the x -component, and w is the z -component of \vec{u} , and we have that $\vec{g} = g(\sin(\alpha), -\cos(\alpha))$, where α is the angle of the track from the horizontal

Writing the Stokes equations component-wise yields

$$u_x + w_z = 0 \quad (3)$$

$$-\nu(u_{xx} + u_{zz}) + \frac{P_x}{\rho} = g \sin(\alpha) \quad (4)$$

$$-\nu(w_{xx} + w_{zz}) + \frac{P_z}{\rho} = -g \cos(\alpha) \quad (5)$$

Nondimensionalizing this model by the choice of

$$x = LX, z = HZ, u = \bar{u}U, w = \bar{w}W, P = \bar{P}p$$

L, H, \bar{u}, \bar{w} , and \bar{P} - the x -length scale, z -length scale, x -velocity scale, z -velocity scale, and pressure scale, respectively— represent constants with dimension that are used to nondimensionalize our model. Since our model is a thin film model, we can assume our height scale is much smaller than our length scale down the track so $\epsilon = H/L \ll 1$, the following system of equations is obtained:

$$u_x + w_z = 0 \quad (6)$$

$$-\nu u_{zz} = g \sin(\alpha) \quad (7)$$

$$\frac{P_z}{\rho} = -g \cos(\alpha) \quad (8)$$

Further, the surface of the fluid, $z = h(x, t)$, obeys the free boundary condition

$$h_t + uh_x = w \quad (9)$$

In the thin film limit, we can ignore surface tension. Additionally, we ignore air induced stress as it is negligible. Following no slip, no surface stress, and by measuring pressure relative to P_{atm} , the following relations are determined

$$u(z=0) = w(z=0) = 0 \quad (10)$$

$$u_z(z=h) = 0 \quad (11)$$

$$P(z=h) = 0 \quad (12)$$

Then the equations above can be solved to obtain

$$P = (h - z)g \cos(\alpha) \quad (13)$$

$$u = \frac{g \sin(\alpha)}{\nu} \frac{hz - z^2}{2} \quad (14)$$

$$w = \frac{g \sin(\alpha)}{2\nu} h_x z^2 \quad (15)$$

Now we consider conservation of mass of the fluid along the track. Let l be the width of the track (y -direction), and let $x = a$ and $x = b$ be planes along the length of the track (x -direction). Since the rate of change of fluid volume between $x = a$ and $x = b$ is defined also as the volume flux going in at $x = a$ minus the volume flux going out at $x = b$, we have:

$$\frac{d}{dt} \left[l \int_a^b h(x, t) dx \right] = l \int_0^{h(a,t)} u(a, z, t) dz - l \int_0^{h(b,t)} u(b, z, t) dz \quad (16)$$

$$l \int_a^b h_t(x, t) dx = l \int_a^b -\frac{\partial}{\partial x} \int_0^{h(x,t)} u(x, z, t) dz dx \quad (17)$$

We assume that h_t and $\frac{\partial}{\partial x} \int_0^h u dz$ are both continuous. Thus it must hold point-wise so we have the following relationship:

$$0 = h_t + \frac{\partial}{\partial x} \int_0^h u dz \quad (18)$$

By nondimensionalizing Equation 14, $u = (hz - z^2)/2$, we find that our governing equation is

$$0 = h_t + \left(\frac{1}{3} h^3 \right)_x \quad (19)$$

The internationalized initial conditions for our system are given by Figure 1.

$$h(x, t=0) = \begin{cases} 0 & \text{if } x < -1 \\ 1 & \text{if } -1 < x < 0 \\ 0 & \text{if } x > 0 \end{cases} \quad (20)$$

Assuming that h is smooth (thus $0 = h_t + h^2 h_x$) and using characteristic curves $X'(t) = h^2$, we can find the shocks in our system.

Our initial shock occurs at time $t = 0$, which is when the fluid starts flowing down the slope. At this shock the front of the fluid is going in to space that initially has no fluid. To find the speed of this shock we use the Rankine-Hugoniot condition.



Figure 2

The Rankine-Hugoniot condition states that for a quantity q that satisfies an equation of the form

$$q_t + f(q)_x = 0 \quad (21)$$

when we have a discontinuity in q , the speed of the shock at that discontinuity is:

$$\frac{d}{dt}s = \frac{[f(q)]}{[q]} \quad (22)$$

where $[f(q)]$ denotes the jump in the function and $[q]$ denotes the jump in the quantity at the discontinuity (i.e. $[q] = q_r - q_l$, where q_r is the value of q to the right of a discontinuity and q_l is the value of q to the left of the same discontinuity). We can apply the Rankine-Hugoniot condition because we have a discontinuity in the height of the fluid and our formula for the height of our fluid (19) satisfies formula 21. The Rankine-Hugoniot condition tells us:

$$\frac{d}{dt}s = \frac{[h^3/3]}{[h]} \quad (23)$$

looking at time $t = 0$ and $x = 0$ we find that the shock speed is $\frac{d}{dt}s = 1/3$. Thus the position of our front for some time after the fluid starts flowing is given by the equation:

$$s(t) = \frac{t}{3} \quad (24)$$

Now consider the rarefaction fan that corresponds to the area where the fluid was present in the left image of Figure 2 and is no longer present in the right image of Figure 2.

The rarefaction begins at $(t, x) = (0, -1)$ so we want to find some solution to our height equation that is of the form $h(\eta = \frac{x+1}{t})$. By taking the derivative of $h(\eta)$ with respect to x and t , and using our general equation for the height (equation 19), we obtain:

$$h'(\eta)(-\eta + h^2) = 0 \quad (25)$$

Thus the rarefaction fan takes the form

$$h = \left(\frac{x+1}{t} \right)^{1/2} \quad (26)$$

Finally, to find the long term behavior of the front of the fluid, we want to find the equation of motion of the second shock where the rarefaction meets the first shock. Our first shock represents the front of the fluid after it starts to flow so this second shock speed will be the new, long term speed of the front.

The time and position at which the first shock and the rarefaction fan meet to create the second shock are $t = 3/2$ (by Equation 24 and 26, $t - 1 = t/3$) and $h = 1/2$ ($t = 3/2$, $x = t - 1 = 1/2$).

Again using the Rankine-Hugoniot condition and solving the differential equation involving the shock speed with the initial condition $s(3/2) = 1/2$, we find:

$$s(t) = (3/2)^{2/3}t^{1/3} - 1 \quad (27)$$

Thus, for a clear fluid without particles, we expect that the position of the front (with constants a and b) after some time should be of the form:

$$x(t) = at^{1/3} + b \quad (28)$$

Now let's consider the movement of particles in the particle laden fluid. It is worth noting that the following section follows a single particle type mixed in fluid. However, in our experiments, we used two types of particles, where our concentration of particles, ϕ , was the sum of the concentrations of particles. For further reading, view [8]. The particles experience the force of gravity, buoyancy, drag, and also shear— due to the velocity gradients the particles are pushed upwards. We will assume that the particles reach terminal velocity (in the z -direction, as indicated by Figure 1) quickly- the time is negligible. We will also follow the Krieger-Dougherty [10] model of effective viscosity, μ (i.e. the effective viscosity increases as a function of the concentration). By this model, μ is a function of fluid viscosity, μ_0 , concentration of particles, ϕ , and the max packing fraction, ϕ_m (the maximum possible particle concentration for randomly packed spheres, determined to be $\phi_m \approx .64$)

$$\mu = \frac{\mu_0}{(1 - \phi/\phi_m)^2} \quad (29)$$

The gravitational force is $F_g = m_p g$, where the mass of the particle (m_p) can be determined by $m_p = \rho_p V = \rho_p \pi d^3/6$, where V is the volume, d the diameter, and ρ_p the density of the particle. I.e., the force by gravity is

$$F_g = \rho_p d^3 g \frac{\pi}{6} \quad (30)$$

The buoyant force is similarly determined:

$$F_b = -m_f g = -\rho_f d^3 g \frac{\pi}{6} \quad (31)$$

With μ being the viscosity and u being the velocity, the drag force is:

$$F_d = 3\pi d \mu u \quad (32)$$

Once at terminal velocity, $u = u_{terminal}$, the net force must be equal. By equations 30, 31, and 32,

$$3\pi d \mu u_{terminal} + \rho_f d^3 g \frac{\pi}{6} = \rho_p d^3 g \frac{\pi}{6} \quad (33)$$

$$u_{terminal} = (\rho_p - \rho_f) \frac{gd^2}{18\mu} \quad (34)$$

Due to hindered settling, additional settled particles make it harder for other particles to settle (for further reading on the settling of particles, see [11]). With the hindrance function $1 - \phi$, we let the terminal velocity be

$$u_{terminal} = (1 - \phi)(\rho_p - \rho_f) \frac{gd^2}{18\mu} \quad (35)$$

Since this is per particle, we now define a particle-volume flux by $\phi\vec{u}_0$, where \vec{u}_0 is a vector with magnitude of the settling velocity, u_0 . For an angle α , and coordinate system defined still by Figure 1. Thus, gravitational settling causes a particle volume flux of

$$\vec{J}_g = -\phi(1 - \phi)(\rho_p - \rho_f) \frac{d^2}{18\mu} \begin{pmatrix} g \sin(\alpha) \\ -g \cos(\alpha) \end{pmatrix} \quad (36)$$

If we let the shear rate be $\dot{\gamma}$, then by [12], the particle volume flux by shear migration is

$$\vec{J}_s = -\frac{d^2}{4} \left[K_c \phi \begin{pmatrix} (\dot{\gamma}\phi)_x \\ (\dot{\gamma}\phi)_z \end{pmatrix} + \frac{K_v \phi^2 \dot{\gamma}}{\mu(\phi)} \mu'(\phi) \begin{pmatrix} (\phi)_x \\ (\phi)_z \end{pmatrix} \right] \quad (37)$$

With K_c , K_v experimentally determined constants. Now we have a conservation law for the particles; the change in concentration should balance the divergence of particle volume flux—consisting of flux due to movement in the fluid, $\phi\vec{u}$, plus flux due to shear, J_s , plus the flux due to gravity and buoyancy, J_g .

$$\phi_t + \nabla \cdot (\phi\vec{u}) + \nabla \cdot \vec{J}_s + \nabla \cdot \vec{J}_g = 0 \quad (38)$$

By shear induced migration, particles migrate from areas of high viscosity to low viscosity. Also, as ϕ increases, the difference of collisions that neighboring particles experience also increases, with more collisions occurring towards the surface of the fluid. Since the density is now a function of ϕ , we have that

$$\rho(\phi) = \phi\rho_p + (1 - \phi)\rho_f \quad (39)$$

Also, since the viscosity is not constant, we let $\tau(\phi)$ represent the viscous stress tensor. Then the incompressible Stokes equations give

$$\nabla P - \nabla \cdot \tau(\phi) = \rho(\phi)\vec{g} \quad (40)$$

Although the velocity of the slurry, \vec{u} , isn't well defined because the slurry consists of both particles and fluid (and the particles move within the fluid), we still have the divergence is 0 by incompressibility. That is,

$$\nabla \cdot \vec{u} = 0 \quad (41)$$

Additionally, with the thin film assumptions, we have that many terms can be neglected due to relative magnitude. Also we can ignore the particle fluxes by an equilibrium assumption, assuming the distance required to reach equilibrium in the z -direction is much smaller than the overall length scale, L . The flux in the x -direction is dominated by the flux in the z -direction. Since there is no flux through the surface of the track nor through the surface of the fluid, the flux in the z direction is zero to leading order so we have an equilibrium distribution in the z -direction. By conservation of fluid and particles, we have the following boundary conditions:

$$u_z(z = h) = 0 \quad (42)$$

$$P(z = h) = 0 \quad (43)$$

From conservation of fluid and particles, we can modify equation 19 to obtain:

$$h_t + (h^3 f(\bar{\phi}))_x = 0 \quad (44)$$

$$(h\bar{\phi})_t + (h^3 g(\bar{\phi}))_x = 0 \quad (45)$$

Where $\bar{\phi}$ is the average depth concentration. The equations derived are solved in [13] for the dynamic model, and in [14] when ϕ is near ϕ_m , with the solution

$$x = Ct^{1/3} + T_0 + O(t^{-1/3}) \quad (46)$$

for C, T_0 constants. Further, for the case of bidisperse, a similar result follows from [8]:

$$x \sim Ct^{1/3} \quad (47)$$

plus some negligible terms.

In both initial conditions that we are interested in (constant volume and constant flux) some qualitative features about the slurry can be explained. It is worth noting that there are regimes where either gravity is the leading force, or shear induced migration overcomes gravity. These situations lead to the settled and ridged regimes, respectively.

The total concentration of the particles and the angle of the track both determine which regime our fluid will be in. As found in [9], we expect a ridge at the front of our fluid at large α and ϕ . As the angle of the track increases, the component of gravitational force that is perpendicular to the track (and induces settling) minimizes and the shear induced migration increases because the higher angle allows the particles to migrate over already settled particles. Conversely, we expect our fluid to be in the settled regime for small α and ϕ . While this is only true for a single particle species, we expect it to be true for the bidensity case. In the settled regime and in the case of bidensity fluids, we expect to see three distinct fronts: one particle front with the higher density particles that settles higher up the track, a second particle front with the lower density particles that settle further along the track, and a third fluid front that is the furthest down the track. As the angle of the track decreases, the perpendicular component of gravity that induces settling increases and it becomes harder for the particles to migrate due to shear. Also, for these small concentrations, the shear decreases even more because there are less particles that can potentially bump into each other and induce migration. The third threshold regime is termed the well-mixed regime. In this regime, we see neither a ridge at the front of our fluid nor particles settling behind the fluid front. The particles seem to stay well mixed within the fluid and, in general, we expect to see this regime at intermediate values of ϕ and α .

We expect to find some intermediate critical concentration that distinguishes the three regimes. Murisic et al. [13] finds a critical concentration which distinguishes the three regimes for the case of monodisperse mixtures:

$$\phi_{crit} = \min \left\{ \phi_m, \frac{-\rho_f(B+1)}{2(\rho_p - \rho_f)} + \sqrt{\left(\frac{\rho_f(B+1)}{2(\rho_p - \rho_f)} \right)^2 + \frac{\rho_f B}{\rho_p - \rho_f}} \right\} \quad (48)$$

Where

$$B = \frac{2(\rho_p - \rho_f) \cot(\alpha)}{9\rho_f K_c} \quad (49)$$

In the monodisperse case, particle concentrations above this critical concentration will lead to a ridged regime while particle concentrations below it will lead to a settled regime. With concentration near the critical concentration, a well-mixed regime is expected, where neither a ridge forms nor separation occurs. We expect a similar result for the bidensity case, where the total concentration is considered.

Now we want to find an equation that describes our clear fluid when we have constant flux instead of constant volume. Our initial conditions in Equation 20 become:

$$h(x, t = 0) = \begin{cases} 1 & \text{if } x < 0 \\ 0 & \text{if } x > 0 \end{cases} \quad (50)$$

In this case we will still have a first shock as the fluid starts to flow down the track. Only the initial conditions have changed so we still expect the speed of our first shock to be the speed found in equation 24. For constant flux, we do not expect to see a rarefaction fan so we also do not expect to see a second shock. Thus we expect that the relationship between the position of our fluid front and time is linear.

When we add particles, we get two different results from the two distinct regimes. In the settled regime, the particles settle while the fluid front continues to move so we basically have clear fluid flowing down the track. We expect to see the same linear relationship between the position of our fluid front and time (this result is also found in [15]):

$$x = Ct + T_0 \quad (51)$$

where C and T_0 are both constants.

In the ridged regime, the result deviated slightly from Equation 51. This is due to the particles that form the ridge of the fluid perturbing the speed of the front of the mixture but we still expect something similar to a linear relationship. Thus, in the case of the ridged regime for constant flux we expect:

$$x \sim Ct \quad (52)$$

3 Experimental Procedure

We conducted two types of experiments, one with a constant volume of fluid and one with a constant flux of fluid with the use of a pump. We used two different particles, white glass beads and the red/white ceramic beads in all of our experiments. This section notes the materials and apparatus used in our experiments, set-up of our track, how we obtained our mixture of fluid and beads, different setups of the camera required for varying analyses, the set up of the pump, and the calculation of the flow rate.

3.1 Materials and Apparatus

3.1.1 Materials

The fluid we used is called Polydimethylsiloxane (PDMS). PDMS has density $\rho_f = 0.971 \text{ g/cm}^3$ and kinematic viscosity $\nu = 10^{-3} \text{ m}^2/\text{s}$.

The two different particles we used, manufactured by Ceroglass, were GSB-7 glass beads with density $\rho_1 = 2.5 \text{ g/cm}^3$ and diameter ranging between 0.18 - 0.25 mm and SLZ-2 ceramic beads which have a density of $\rho_2 = 3.8 \text{ g/cm}^3$ and diameter ranging between 0.125 - 0.25 mm. We used an OHAUS-Scout pro scale to measure the mass of the beads and the fluid used in each experiment.

name	diameter	density	color
GSB-7 glass beads	0.18 - 0.25 mm	2.5 g/cm ³	white
SLZ-2 ceramic beads	0.125 - 0.25 mm	3.8 g/cm ³	red

3.1.2 Track

The apparatus we used was an plastic track with an angle that was adjustable with respect to the ground. Experiments were run at angles of 20° and 50° . Changes in the angle of the track were made manually by moving the track along the two, tilted metal bars to which it is fixed. To ensure precision in the angle, we used a protractor and then a spirit level laid horizontally to eliminate unevenness.



Figure 3: This image shows the apparatus used in our experiment placed at 50° . The right side is connected to two metal supports by which the angle of the track (the black platform) can be altered.

3.1.3 Laser

A green Class II laser sheet was used in all experiments that involved obtaining height profiles of the fluid as it traveled down the track. The laser was set up in such a way for the beam to be parallel to the longer side of the track. All light sources were turned off while conducting these runs to decrease the noise captured by the camera while the experiment was in progress.

3.1.4 Camera

For all of our runs, we used a Canon EOS Rebel T2i camera. When pouring the fluid down the track for front tracking analysis, we tried to find the best angle and position to set up the camera in order to get the best data for our code. Within a week of running the experiments, we realized that setting up the camera to be parallel to the track (the angle of the camera was the same as the angle of the track) gave the best results in terms of our front position analysis. For height analysis, we found that it was best to angle the camera in a way to get a good visual on both the vertical and horizontal perspective of the track (this will be explained in more detail further in Section 3.2). A tripod was used to allow the camera to capture these various positions. The camera was always placed approximately half a meter away from the track and the camera was focused so that the fluid flowing down the slope was in focus. For height analysis, the camera was positioned to one side of the track so that the laser line was horizontal on the camera screen.

3.1.5 Pump

We used a Mityflex 4200 pump in our constant flux experiments. There are two controls on the pump. One of the controls is used to change the direction of the flow. By switching the control to be either clockwise or counterclockwise, we can choose the direction of the flow. The other control is used to adjust the flow rate and has a scale of 2.5% to 100%. However, the actual flow rate depends on many other aspects, for example, the volume fractions and the viscosity of the fluid. As viscosity and volume fraction are increased, the flow rate decreases. At a high volume fraction, the fluid left the pump in pulses rather than continuously pouring out. For this reason, we added a weir on the top of the track to allow the fluid to flow down the track smoothly.

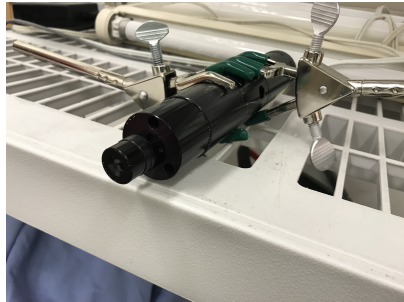


Figure 4: Laser



Figure 5: Camera



Figure 6: Pump

3.2 Procedure

We divided these experiments into several steps: the preparation of fluid, track setup, the measurement of the actual flow rate, front tracking experiment, and laser height profile.

3.2.1 Preparation of PDMS and Particle Mixture

We first need to prepare our particle mixtures with given concentrations. To prepare the fluid with appropriate concentration of two types of beads, we first calculated the theoretical weight of PDMS for a given volume. Then we measured a certain amount of PDMS according to our calculation above. In general, we have the formulas:

$$\phi_1 = \frac{V_1}{V_1 + V_2 + V_f}$$

$$\phi_2 = \frac{V_2}{V_1 + V_2 + V_f}$$

ϕ_1 represents the volume fraction of the concentration of the glass beads, ϕ_2 represents the concentration of the ceramic beads, V_1 represents the volume of glass beads, V_2 represents the volume of ceramic beads and V_f represents the volume of PDMS.

Given the concentration of two different beads and the total volume of the fluid, which is also the volume of the PDMS, we can now calculate the weights of glass beads and ceramic beads separately by solving the formula above.

$$m_1 = \frac{\phi_1 \rho_1 m_f}{(1 - \phi_1 - \phi_2) \rho_f}$$

$$m_2 = \frac{\phi_2 \rho_2 m_f}{(1 - \phi_1 - \phi_2) \rho_f}$$

3.2.2 Track Setup

In order to start our experiments, we first made sure that the track had no fluid residue from previous experiments so that our front tracking or height experiment would have a lower error.

To set up the track in the angle we want, we first lifted the track to an approximated angle. Then, we used the protractor to measure the angle along the longer side of the track. We kept adjusting the angle until we got the desired angle on both sides of the track. Next, we checked the balance of the track by using the level. In addition, we need to check the balance and the angle after each run if we are doing multiple runs in one experiment to minimize any possible errors in our experiment.

3.2.3 Measurement of Flow Rate

All constant flux experiments were conducted at 20% flow rate and we measured the actual flow rate of our fluid before the experiment. To measure the actual flow rate of the fluid, we first need to calculate the total volume and total weight of our fluid to find out the density of the overall volume.

$$V_{total} = \frac{m_f}{\rho_f} + \frac{m_1}{\rho_1} + \frac{m_2}{\rho_2}$$

$$m_{total} = m_f + m_1 + m_2$$

$$\rho_{total} = \frac{m_{total}}{V_{total}}$$

where m_f and ρ_f represent the weight and density of the fluid, m_1 and ρ_1 represent the weight and density of the glass beads, m_2 and ρ_2 represent the weight and density of the ceramic beads and ρ_{total} represents the density of our mixture.

Then, we turned on the pump, waiting for a few seconds to get rid of the air bubble inside the pipe. After that, we measured the weight of the fluid coming out of the pipe in a certain time interval. The time was measured. Next, we used the density of the mixture to get the actual flow rate (the unit is mL/s , and t represents the time in seconds).

$$\text{Flow Rate} = \frac{m}{t\rho_{total}}$$

We repeated this process four or five times. Finally, we averaged the flow rate and got our actual flow rate.

3.2.4 Front Tracking for Constant Volume

We set up the camera and track such that they were parallel to each other, which meant making sure the angle of the track was the same as the camera lens. We need the lens and track to be parallel for data analysis. We had to make sure the camera was not moved once the experiment started so that our data was not affected by video noise.

To start the front tracking with the constant volume, we made sure the mixture was well mixed and there was no separation between the beads and the PDMS. Then we placed the gate on the track and pour the mixture behind the gate to allow the mixture to start sliding at the same time and not be affected by the time it took to pour. Once the mixture was behind the gate, we started recording and proceeded to quickly remove the gate to allow the fluid to move down the track. We allowed the camera to record until the front of the mixture was almost at the bottom of the track.

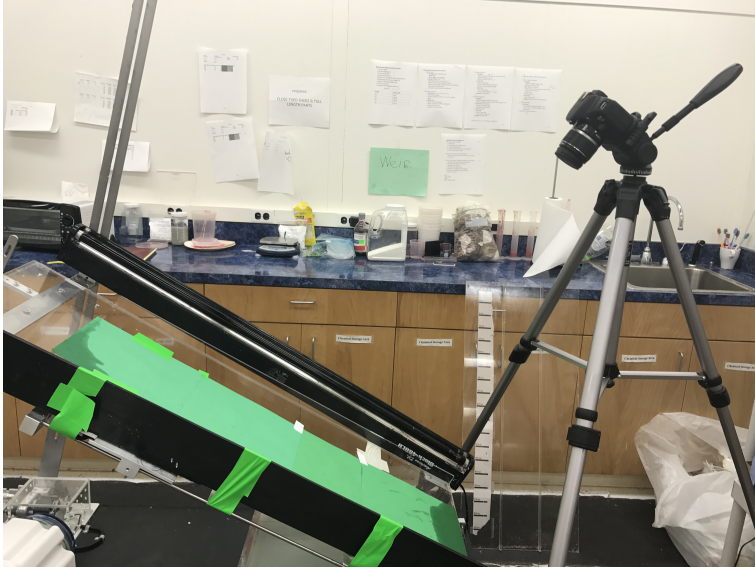


Figure 7: This image shows the position of the camera with respect to the track.

3.2.5 Front Tracking for Constant Flux

For constant flux experiments, we set up the camera like we did in the constant volume experiments. The camera should be as parallel to the track, suggesting the angle of the camera lenses should be the same as the angle of the track. Before starting the front tracking with constant flux, we first made sure that the

fluid was well mixed and the control of the pump was turned to 20%. Next, we need to let the pump run for a few seconds to make sure that there were no air bubbles left in the pipe and then calculated the actual flow rate as described in section 3.2.3. Next, we need to place the weir at the top of the track to smooth the mixture.

To start the experiment, we put the output pipe behind the weir. One person was needed to mix the fluid before it flowed over the weir to make sure that the fluid is evenly distributed on the track. Once the mixture passed the weir, we started recording. During the experiment, we need to constantly stir the mixture to ensure that our fluid is well-mixed in the pump.

3.2.6 Height Profile Experiments

For the laser height profile experiment, we used the camera to record a laser line that was incident on track and our fluid. For the experiment, we first adjusted the position of the laser so that the laser line is positioned in the middle of the track and is parallel with the length of the track. We also changed the angle and position of the camera so that the video can catch most of the track. Furthermore, the angle of the camera was almost the same as the angle of the track so that the laser line would be a horizontal line in the image.

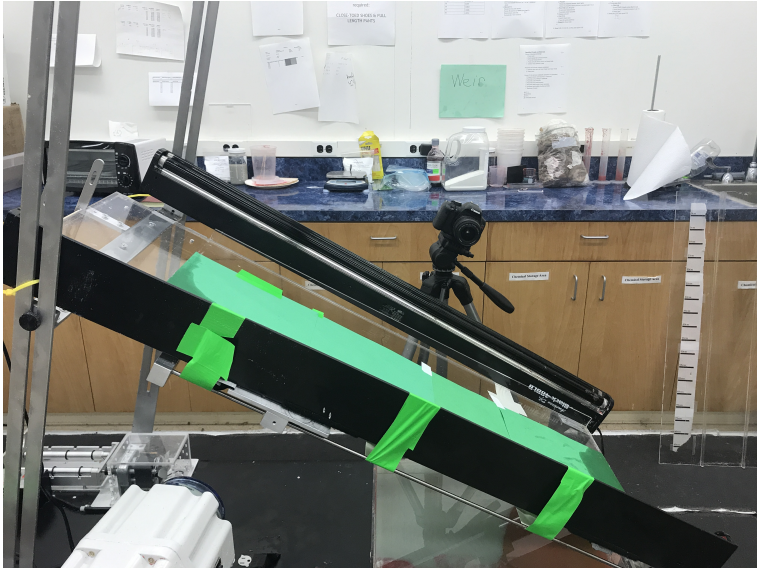


Figure 8: This image shows the position of the camera with respect to the track for the laser height profile experiment.

Next, we took the screen shots of the video and used Matlab to analyze the data by comparing the images taken from the video with a calibration image. Generally, we used a coin (with height 2 mm) or a ruler (with height 6 mm) as calibration objects. We first turned off all light sources. Then, we turned on the laser and recorded the laser line with the calibration objects as a reference. After that, we started the experiment as we did in the front tracking with the laser.

4 Data Analysis

After collecting the video data, we use Matlab to analyze our results. Programs are written for both the front tracking and height profile experiments. Both programs have a set of protocols for the user to follow in order to properly and efficiently run the code and reduce instances of user error.

4.1 Front Tracking

In order to run the front tracking script smoothly, the user must satisfy certain criteria. The relevant Matlab files must be present in the current working directory, along with two additional folders named **Frames** and **Output** (Figure 9). **Frames** must be empty. **Output** must be empty except for the video that is going to be processed, which must be named `video.mov` or `video.MOV`. The primary script for front tracking, named `FrontTrackingScript.m`, calls the necessary scripts and functions so the user is not required to call them manually.

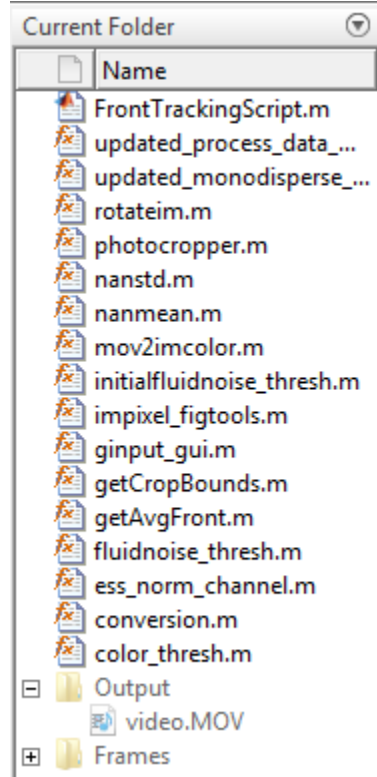


Figure 9: The 17 files used in Front Tracking are all together in the current folder directory, along with the folders **Frames** and **Output**.

Once the initial conditions are satisfied, the user runs the program. The user is prompted for a start time, an end time, and a time interval between frames, also called the time step. The user must watch the video to choose the appropriate values of the variables so as much of the video as possible is processed while avoiding possible issues in the video such as reflections or blurriness, also called noise. The program then extracts the frames and saves them into **Frames**.

After the frames are extracted, `FrontTrackingScript.m` calls `photocropper.m`. The images need to be oriented with the bottom of the track pointing to the left size of the screen, but are currently pointing to the bottom of the screen. The user is prompted to select a point at the top of the track, along the actual wall of the track, a point at the bottom of the track, and also a point along the wall. These points should be on the wall to ensure that they are in the same direction of the track. Then, the program calculates the angle between the points and rotates the images the appropriate amount.

The user is prompted to select the measurement lines and the top and bottom bounds of the track along the rotated image, as well as the left and right bounds of the track (Figure 10). The user should choose the bounds of the track so they include only the track, and no area outside of the track to reduce noise. If

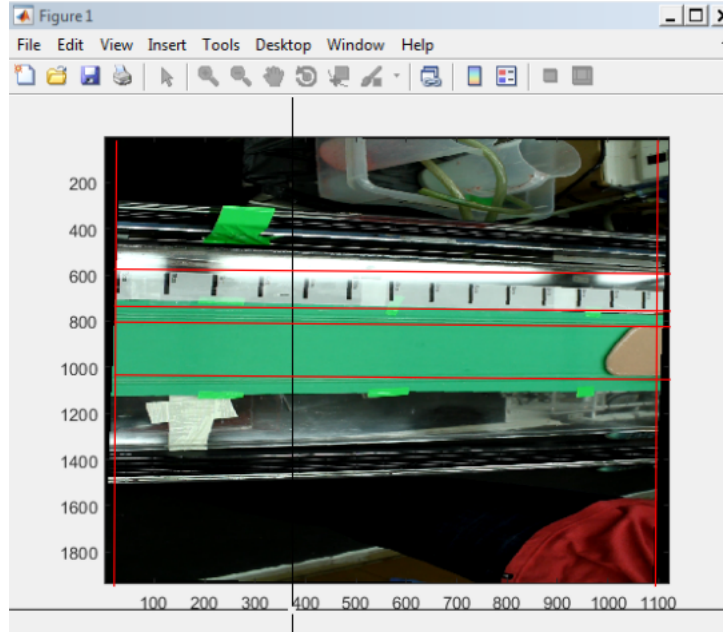


Figure 10: This is the displayed image shown in photocropper.m. The red lines show good approximate choices for the bounds of the track and the measurement lines.

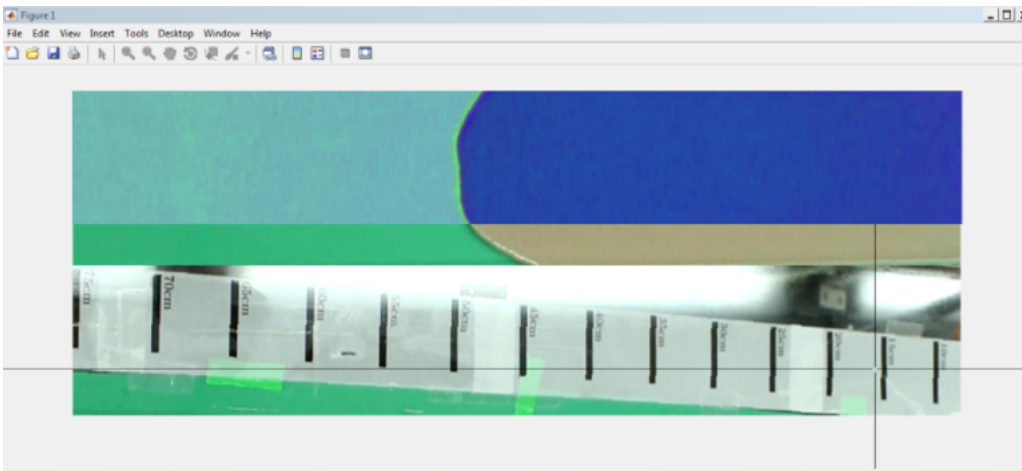


Figure 11: The above image shows the two displayed images for choosing points on the fluid's fronts and the measurement lines, but spliced together. The inverted color scale portion is for choosing points along the fronts, while the regular color scale image is for choosing points along the measurement lines.

there are obvious sources of noise inside the track, the user should avoid those points if possible. However, if the user crops too much, the fronts may go past the chosen boundaries before the end time and the program will assume that the front stopped moving. The measurement lines are chosen more liberally, selecting more rather than less of the boundaries, though the bottom of the measurement boundary should not pass the top of the track boundary. After this program, the frames are cropped and saved into the `Frames` folder. `photocropper.m` takes the cropped measurement lines and puts them at the bottom of the track boundaries, saving them together as a single photo (Figure 11).

The last function `FrontTrackingScript.m` directly calls `updated_monodisperse_processor.m`. This function's purpose is to collect the information that will be used to determine where the average position of

the front is in the frame at every time step. The user is prompted to choose the number of times they wish to run this function. The more times this function is run, the greater degree of accuracy the plots will have once they are made. For more information on why this occurs, refer to Section 4.3.1.

First, the program prompts the user to choose points along the measurement line to convert pixels to centimeters. The program will output the non-color-inverted image (Figure 11), and the user selects each line from right to left. The points selected are approximately the same point on each line, e.g. being chosen on the top left or bottom right portion of the line. This section is only done once within `updated_monodisperse_processor.m`. Then, the user selects points for both fronts, either for two particle fronts for settled experiments or both for the same front in ridged experiments. This selection process is repeated for however many times the user previously chose to run the function. These points are selected from the inverted color scale image (Figure 11) so the different fronts are distinct from each other.

Using the mouse, the user selects points for each run. If `updated_monodisperse_processor.m` is being run only once, the user selects about 20 points for both fronts. If it is being run multiple times, the user selects 5 to 10 points, since choosing points along the fronts takes time. The selected points should be at the front most edge, and in the case of no separation when there is only a single front, then the user chooses points for the same front twice. The program saves the maximum and minimum value for the color of the front to determine the position.

Within `updated_monodisperse_processor.m`, `updated_process_data_monocolor.m` is called. This function determines the average front position against time. This function is run the number of times the user chose to run `updated_monodisperse_processor.m`, and a vector containing the position and time for each specific run is saved. To do this, the program uses the maximum and minimum color value. It checks along horizontal planes within the images to find where the front is. The program saves processed images with dots along the fronts, as well as the time, α , and ϕ values, which are prompted from the user.

Lastly, within `FrontTrackingScript.m`, the program produces a video and plots. The video is made using the processed images in `Frames` that have the time stamp and dots along the front, so users can see the progression of the front with time, as well as noise within the image. `FrontTrackingScript.m` creates vectors with the average position and standard deviation using the position vectors made from `updated_process_data_monocolor.m`. From these vectors, a position plot with error bars, a velocity plot, and log plots of position and velocity are made and saved to `Output`.

There are three log plots made. Two plots are the loglog plots that take the log of time on the x-axis and the log of either the position or velocity on the y-axis. These graphs also have the idealized plot on the graph for comparison. For position, the idealized line has a slope of $1/3$, since the motion should be dependent on $t^{1/3}$. For velocity, the idealized line has a slope of $-2/3$, since the velocity should be dependent on $t^{-2/3}$. The last plot is the position and time along with a best fit line.

4.2 Height Profile

To run the program for the height profile experiments, the user must have the files `UpdatedLaserHeightScript.m`, `laserHeightCalibration.m`, and `laserHeight.m` in the working directory. This directory should also contain the video of the experiment named `video.mov` and empty folders called `OutputVects` and `OutputPics`.

The program prompts the user to input the incline angle of the track, and the concentrations of the different types of particles. Then the program tells the user to, "Input the time (in seconds) of lights on with the ruler on the track." This is the time in seconds which corresponds to the frame of the video with the ruler flat on the track with the lights on, so that the tape is visible. Similarly, the program prompts the user to "Input the time (in seconds) of lights off with laser on calibration object" and "Input the time (in seconds) of the reference laser line". These correspond to the frames with the laser on top of the ruler in the

dark (calibration image) and the frame with the laser on the empty track (reference image), respectively.

Next, the user is shown a picture of the calibration image superimposed on the reference image. The user crops the image as close to the lasers as possible, and then select the points on the x-axis where the ruler starts and ends in the picture.

Finally, the user is prompted to enter the start time for the data. This corresponds to the time (in seconds) in the video in which the fluid enters the frame. Similarly, the user is prompted to enter the end time for the data, which is the time that the front of the fluid leaves the frame. Lastly the user is asked to “Input the seconds between frames.” This is the number of seconds between each frame that the program uses to generate height graphs. For example, if the user enters 1, the program will generate a height graph every second between the time the fluid front enters the frame and the time it leaves the frame.

The program creates a video called `Height_Video.avi`, which is a video of all the height graphs. All the individual graphs are saved in the `OutputPics` folder. A matrix of all the heights, a matrix of all the positions, and a vector of all the corresponding times are stored in the `OutputVects` folder.

4.3 Error

Our results have three general sources of error, human error, experimental error, and computational error. When analyzing data we are concerned with the computational error, which could be a result of bugs in the code or roundoff error in some of the variables when running the code.

4.3.1 Front Tracking

One source of error is that the mass of all objects is within a $0.1g$ of its actual value, however, this can be neglected as all quantities had mass $m \geq 15g \gg 0.1g$. A reasonable source of error is that some of the fluid mixture was still left in the container, and did not enter the track. In some runs, when we used two different containers to make separate slurries and then mixed them, we would lose some of one mixture, resulting in different concentrations than calculated. However in later runs we began making the mixture in only one container to eliminate this error.

When pouring our mixture (which consists of a designated mass of glass and ceramic beads along with a certain amount(usually 80 mL) of PDMS), we attempted to pour out as much of the liquid as possible from the container and onto the track. However, there was always some mixture remaining in the container. Furthermore, at times some of it dripped onto the track from the spatula (what we used to help pour) or seeps over the walls of the gate. After the first run, while we attempted to clean the track to the best of our abilities, some PDMS remained stuck on the plastic surface. We reused our mixture for all runs, and since we are unable to calculate the mass of the unused mixture that never left the container, we are therefore unable to account for the mass of each particle and fluid lost. This caused the concentration of particles in the “new” fluid to be unknown (since we don’t know exactly how much particle and fluid volume we lost). So in runs following the first one, while we can estimate the concentration of particles in PDMS, we do not know what it actually is. Any fluid left on the track after the cleaning process might also result in error as it could alter the motion of the fluid in the new run by means of reducing/increasing fingering or altering the behaviour of the fluid front and its velocity down the track.

Another source of error we have encountered is precision in angling the track to be perfectly equal on both sides. We have had many runs in which while flowing down the track, the fluid leads on either the right or left side as opposed to having its leading point to be centered as one would assume. Although we use a protractor along with a spirit level as an attempt to get the angle as accurate as possible, the track may still end up slightly tilted to one side by a fraction of a degree. Human error could also be a source of why the fluid leads either to the left or to the right. In our runs, a member held the gate and pulls it up to

release the fluid once it is time. This pulling motion is usually directed towards this individual thereby may cause some of the PDMS to drip from the lifted gate and onto the track which may force the fluid to “lead” in that general area.

Another issue we have encountered involves working with the camera and how it captures our images. In some runs (for instance when measuring the height profile) it was important not to touch the camera during the entire run as for we needed to get images of the run happening as well as a captured reference and calibration frames without any shifting of the camera. A slight touch could lead to a fairly large change in perspective. This would make comparing our data to a reference and calibration image much more difficult.

Additionally, the images from the camera get mildly distorted. The portions of the image that are closest to the camera will have mildly different pixel to centimeter or millimeter conversion ratios than portions farther from the camera, since an object farther away will appear slightly smaller. Because of this, the height profile, and to a lesser extent, the front tracking, have errors in their axes measurements, since both programs assume a constant pixel conversion ratio.

For Front Tracking, the last major source of error comes from the programs used for the data analysis. The points the user selects determine the maximum and minimum color values that the program then uses to determine where in the frame the particle and fluid fronts are. Minor differences in selected points can produce drastically different position profiles, but ideally, the program would choose that same profile each time.

To deal with this issue, the program utilizes multiprocessing to run this program, however many times the user specifies. The user selects points on the fronts for each run. This data is all saved, and graphs are produced from the average position profile. The greater number of times the program is ran, i.e. the greater number of samples selected, the more accurate the position profile will be in reflecting the true position profile. These are not random samples, but they ideally will average out any discrepancies made in the point selection. That said, the user must always be careful when selecting points along the front. Any careless point selection can produce a very inaccurate position profile, which will affect the average results.

Additionally, the standard deviation of all the profiles is calculated at every time step. This data is utilized in the position graph. By doing it at every time step, the graph can show individual times when the images lacked a clear front for the program to pick up, i.e. when the particle and fluid fronts begin separating in the settled experiments and the clear color of the particles become more separated and unclear. This example would show larger error bars on the portion of the position graphs that refer to the the portion of the experiment when the fronts are separating (Figure 12).

There can be errors when separation is not occurring as well. Any source of error could interfere with the program when it is determining the location of the front. It is helpful to watch the outputted video to locate the sources causing the error at the specific times when there are large error bars, and re-run the data with new crop bounds, a better time step, or some change that better accounts for the errors and allows the program to have a more accurate position profile.

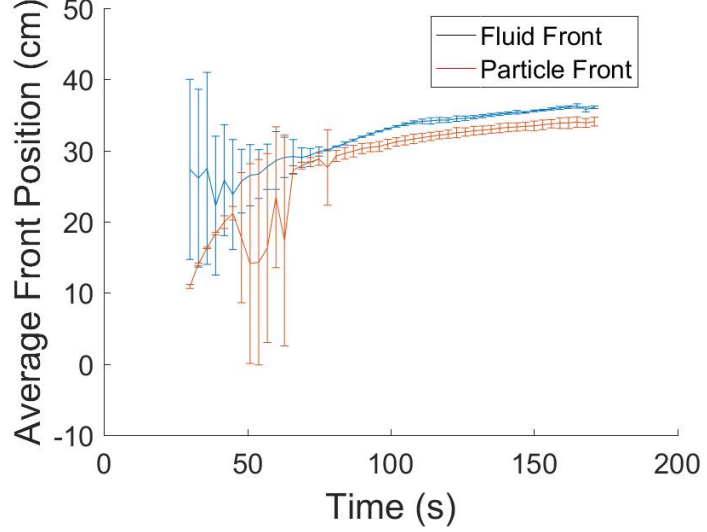


Figure 12: In the above settled regime example, the early portion of the graph shows large error bars, indicating that the program had difficulty distinguishing fronts during separation.

4.3.2 Height Profile

The new height code is fairly accurate. We measured this by running the code using the frame with the ruler not only as the reference picture but also as the data, which outputted the graph below. The actual height of the ruler was measured to be 7.3 mm which the graph represents. However, the graphs generated always have jagged lines regardless of whether we are analyzing the ruler or the actual fluid, suggesting the code is picking up some sort of noise.

5 Results

Consider the different regimes that formed due to changes in the inclination angle, α , of the track and particle concentration, ϕ . As discussed previously in Section 1, there are three possible regimes that can form: ridged, well-mixed, and settled. The ridged regime is identified by a high concentration of particles on the outer edge of the fluid that form a leading ridge. The well-mixed regime is formed when particles stay evenly distributed throughout the fluid. Finally in the settled regime, particles form a sediment at the bottom of the fluid as it flows down the track. As a result, separation between different particles and fluid can be seen. In our experiments, this was visible to the naked eye by dying particles different colors in order to visualize separation, as well as using a front tracking and height profile code to analyze recorded data.

Our results are divided into three major sections: experiments run with a finite volume of fluid, experiments run with a constant flux, and the height profiles of the different regimes. Within these sections, the angle of the track on which the fluid was poured, α , and the volume fraction ratio, ϕ , of glass beads to ceramic beads are discussed. These were the only two parameters that varied with each experiment. As previously mentioned in Section 3.2.1, each individual volume fraction is given by:

$$\phi_1 = \frac{V_1}{V_1 + V_2 + V_f}$$

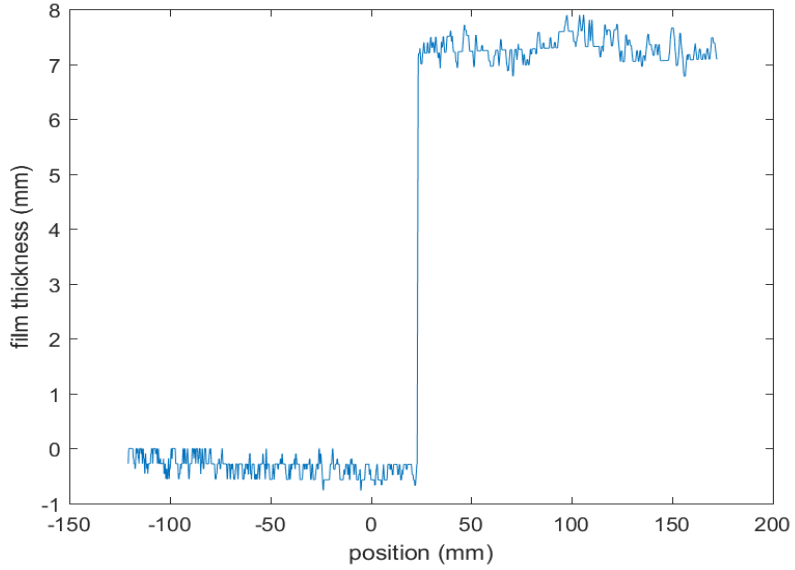


Figure 13

$$\phi_2 = \frac{V_2}{V_1 + V_2 + V_f}$$

We will use χ to present our results where:

$$\chi = \frac{\phi_1}{\phi_1 + \phi_2}$$

Simplifying this expression, we get:

$$\chi = \frac{V_1}{V_1 + V_2} \quad (53)$$

Thereby χ is just the fraction of the volume of glass beads to the volume of both glass and ceramic beads. Each of the regimes mentioned above are specific to the inclination of the track and concentration of particles in the fluid and is also dependent on χ .

5.1 Constant Volume

5.1.1 Front Tracking

Experiments conducted with a finite volume of liquid, typically set to be 80 mL, were carried out at three different χ values (0.389, 0.5, and 0.889) and at two different angles ($\alpha=20$ and $\alpha=50$). General observations about each run can be made upon comparing all experiments at their χ and α values:

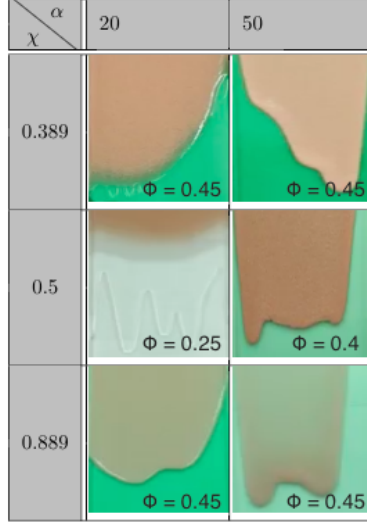


Figure 14: Experiments conducted with a finite volume of fluid moving down a ramp positioned at α degrees and a volume ratio, χ , of particles. Each run's ϕ value is also presented in the bottom right corner of each image. Reference Equation 53 for exact definition of χ .

It is important to note the regime that occurs at each run as well as the total volume fraction, ϕ . With each respective slurry, a higher ϕ represents a higher viscosity.

(χ, α)	(0.389, 20)	(0.389, 50)	(0.5, 20)	(0.5, 50)	(0.889, 20)	(0.889, 50)
regime	settled	ridged	settled	well-mixed	well-mixed	ridged
ϕ	0.45	0.45	0.25	0.40	0.45	0.45

Table 1: The six experiments presented in Figure 14 along with the regime observed and the total volume fraction of the fluid, ϕ , where $\phi = \phi_1 + \phi_2$. Note that the light grey columns are runs that occurred at $\alpha = 20^\circ$, while white columns are at $\alpha = 50^\circ$.

Recall Equation 28 in which we can estimate the position of the front, $x(t)$, of a constant volume of fluid poured down the track after some time, t . After some calculations, remember that we are expecting t to be raised to the one-third power.

χ	0.389	0.5	0.889
20	0.648	0.224	0.242
50	0.309	0.172	0.450

Table 2: The exponent of t obtained through experimentation corresponding to each of the runs shown in Figure 14.

Screen shots of each run in Figure 14 show the difference in slurry behavior based on the angle and increasing volume fraction of particles. Taking a look at $\chi = 0.5$ where volumes of both particles are equal, there is a noticeable difference between the two runs at inclination angles of $\alpha = 20$ and $\alpha = 50$. At $\alpha = 20$ fingering starts nearly at the very beginning of the run and at least four fingers form. Meanwhile at $\alpha = 50$ there is no separation of particles in the slurry and only one small leading finger forms at the left side of the fluid.

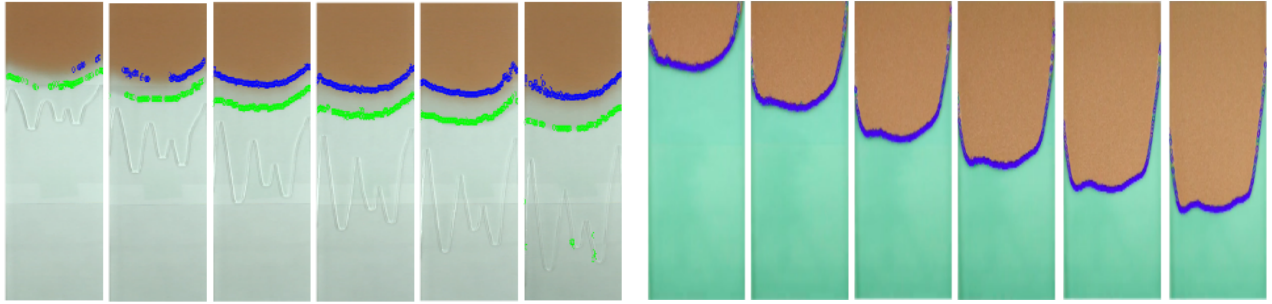


Figure 15: Screenshots obtained from the front tracking code at every 20 seconds of the slurry running down the track at $\alpha = 20^\circ$ and $\chi = 0.5$. The green and blue dots track the front position of the glass beads and ceramic beads, respectively.

Figure 16: Screenshots obtained from the front tracking code at every 12 seconds of the slurry running down the track at $\alpha = 50^\circ$ and $\chi = 0.5$. The green and blue dots track the front position of the glass beads and ceramic beads, respectively.

Figure 15 is a clear example of a settled regime in which there is distinct separation between the front of the PDMS, the front of the glass beads, and the front of the ceramic beads. Given that ceramic beads are more dense than the glass beads, it is not surprising that they are the first to settle to the bottom of the fluid because they have more mass. As the mixture in Figure 15 traveled down the track, ceramic beads sunk to the bottom of the fluid first (led by the blue points) followed by glass beads (led by the green points) and finally a layer of thin film. Meanwhile Figure 16 is an example of a well-mixed regime. Blue and green dots represent each particle's front. They merge together into one fluid front. Consider the average front position plotted against time for both runs:

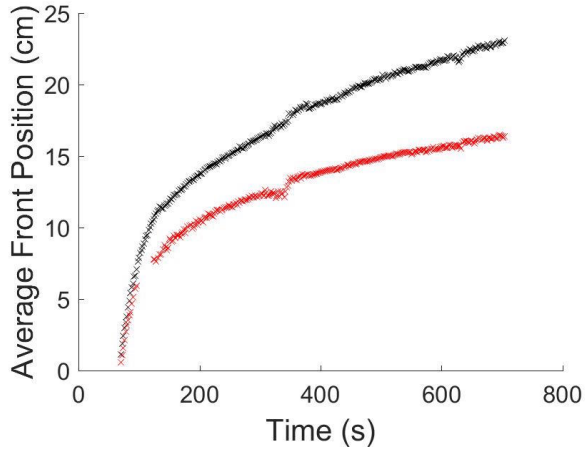


Figure 17: Average front position for $\alpha = 20^\circ$ and $\chi = 0.5$ in which the front of the fluid mixed with glass beads is represented by black dots and the front of the fluid with ceramic beads is represented by red dots.

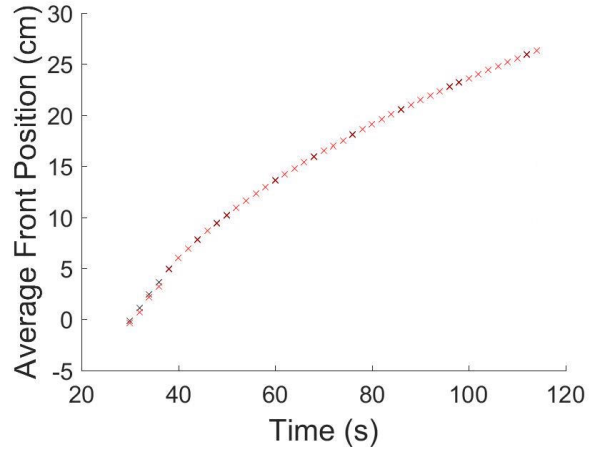


Figure 18: Average front position for $\alpha = 50^\circ$ and $\chi = 0.5$ in which the front of the fluid mixed with glass beads is represented by black dots and the front of the fluid with ceramic beads is represented by red dots.

The purpose of varying the fraction ratio and angle was to compare the different behaviors of the slurry and to study the settled, well mixed, and ridged regimes. From Figure 14, notice a settled regime for an angle of $\alpha=20$ and volume fraction, $\chi=0.389$. Shear induced migration pulls the particles toward the track. Under

the no slip condition (mentioned in Section 2) particles in contact with the track will not slip and thereby will not move with the rest of the fluid. So separation of particles with different densities is more visible.

Taking a look back to Table 2, notice that exponents of t that we obtained from experimental results are all fairly close to one-third, however we see one discrepancy at $\alpha = 20$ and $\chi = 0.389$. This experiment was actually run twice on front tracking so upon closer examination, we were able to examine and compare both runs. The fitted equations to each run are as follows:

$$x = 34.1054t^{0.18098} - 68.4044 \quad (54)$$

$$x = 0.2281t^{0.64828} + 4.1789 \quad (55)$$

Neither run explains the theory we are examining of t having an exponent of one-third after some short amount of time has passed. Both experiments were run on the full data (roughly 600 seconds). Such drastic differences in the fluid's front speed as it flowed down the track may be due to experimental error ranging from not fully wiping down the track causing traces of fluid from previous runs to remain on it to the track being slightly slanted. Looking deeper into these runs, we then decided to also test our data on only the last portion of the run and we chose Run 1 to do so. The fitted equation of this portion of the data is the following:

$$x = 4.7247t^{0.3803} - 13.7983 \quad (56)$$

The t exponent is 0.3803 for the data for the last 200 seconds of the run. What our theory predicts does not correspond to obtained data since roughly the first 400 seconds of the run were eliminated. This shows that the rapidly approaching equilibrium assumption might not be holding.

We can see separations between particles and PDMS in experiments done at an inclination angle $\alpha=20$. For instance in images at $\alpha=20$ for $\chi=0.389$ and $\chi=0.5$ we see settled regimes. Ceramic particles settle down on the track at a slower rate when compared to the glass beads and PDMS. We can see an example of a well mixed regime in the experiment done with a volume fraction ratio of $\chi=0.889$. This slurry is traveling down the track at $\alpha=20$ and no separation is visible to the naked eye. Now take a look at runs conducted at $\alpha=50$. At $\chi=0.389$ and $\chi=0.889$ a ridged regime formed. Notice also that the volume fraction for both these runs is greater than the volume fraction at $\chi=0.5$ ($\phi = 0.45$ vs. $\phi = 0.40$). Perhaps this slightly higher volume fraction is what cause a ridged regime in the first two runs but a well-mixed fluid resulted in the later. At this higher angle, shear induced migration dominates gravitational force which explains the higher concentration of particles at the front of the fluid.

It is discussed in the Section 2 that the front position of our slurry front vs. time can be modeled by Equation 28, which was derived using the Rankine-Hugoniot condition. Although there are minor discrepancies, the majority of our results match the predicted theory of position front.

5.2 Constant Flux

Constant flux experiments were conducted using a pump that constantly pumped the PDMS and particle mixture onto the incline. The approximate volume of fluid used for each experiment were about 500 mL and again, the angle and concentration varied with each experiment. Flow rate of the pump was calculated before each run for reference. Data is presented by the angle of the track, α , and χ .

5.2.1 Front Tracking

Observations about fluid front with constant flux were different from the ones made in experiments with a constant volume of fluid. The behaviour with respect to fingering, separation, and velocity varied by experimental specifications. Experiments conducted with constant flux for front tracking analysis were

conducted at four different χ values (0.376, 0.389, 0.880, 0.889) and at $\alpha=20$ and $\alpha=50$. General observations about each run can be made upon comparing all experiments at the previously mentioned χ and α values:

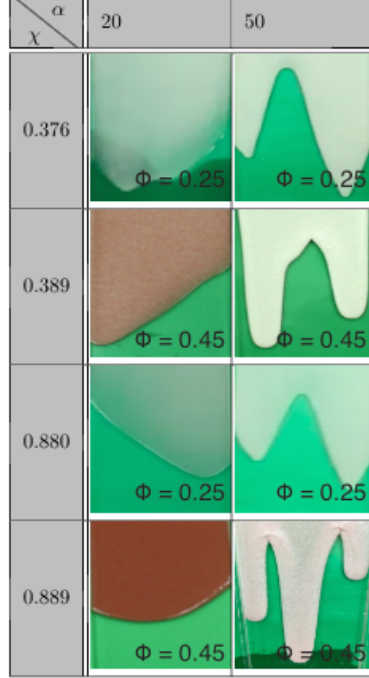


Figure 19: Experiments conducted with a constant flux on a ramp positioned at α degrees and a volume ratio, χ , of particles. Reference Equation 53 for exact definition of χ .

Regimes and volume fractions, ϕ , corresponding with experiments presented in Figure 19:

(χ, α)	(0.376, 20)	(0.376, 50)	(0.389, 20)	(0.389, 50)	(0.880, 20)	(0.880, 50)	(0.889, 20)	(0.889, 50)
regime	settled	well-mixed	well-mixed	ridged	settled	well-mixed	well-mixed	ridged
ϕ	0.25	0.25	0.45	0.45	0.25	0.25	0.45	0.45

Table 3: The six experiments presented in Figure 19 along with the regime observed and the total volume fraction of the fluid, ϕ , where $\phi = \phi_1 + \phi_2$. Note light grey columns are runs that occurred at $\alpha = 20$, while white columns are at $\alpha = 50$.

We expected the front position of the slurry to move linearly with time and therefore for velocity to be constant throughout the run, recall Equation 51. Therefore t should be raised to the first power:

$\chi \backslash \alpha$	0.376	0.389	0.880	0.889
20	0.583	0.830	1.18	0.888
50	1.197	0.819	1.178	1.083

Table 4: Table of exponents of t. Compare to 1 as we expected velocity to be linear.

It was observed that the initial behavior of the mixture on top of the weir would have an effect on the fingering. In our experiment at $\alpha = 20$ and $\phi=0.389$, the slurry went over the weir evenly and did not form

any fingering. This slurry was well-mixed while flowing down the track and no distinguishable separation between the beads was observed. It is important to note that a slight separation between the beads and the PDMS did occur but it was not significant enough for the camera to record and therefore, our code does not take this into account. This slight separation was at the front of the slurry in which a gradient, the length of roughly two millimeters, formed. This scenario might not repeat itself if the volume ratio of the slurry is smaller or the angle is changed.

Now examine runs at same the different inclination angles but same χ and ϕ values ($\chi=0.880$ and $\phi=0.25$):

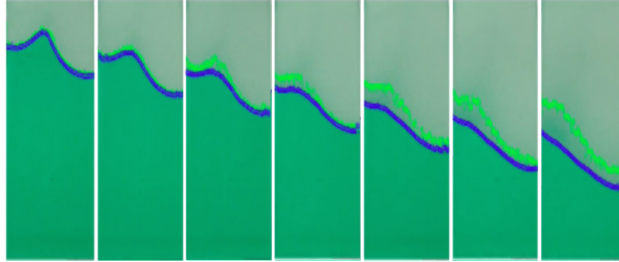


Figure 20: These screen shots are taken at 10 second intervals of the fluid moving down the ramp at $\alpha = 20$ and $\chi = 0.880$.

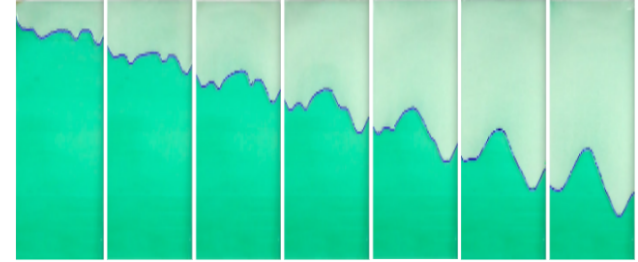


Figure 21: These screen shots are taken at 10 second intervals of the fluid moving down the ramp at $\alpha = 50$ and $\chi = 0.880$.



Figure 22: From left to right, 4 runs conducted at $\alpha = 50$ and $\chi = 0.889$ in which the first two were for front tracking and the last two for height profile.



Figure 23: The image above is a close up of the first run (far most left) of Figure 26, conducted at $\alpha=50$ and $\chi=0.889$. A ridge is visible at the front. The two hill-like sections here are presented as they were 60 cm down the track. Note in this run the weir that acted as a barrier between the slurry and the track, slipped roughly 3 cm during the run.

Constant flux is expected to have a linear front velocity due to the constant pumping of slurry onto the track. This linear trend can be observed in Figure 20 and Figure 21.

In the experiment at which the inclination angle was at $\alpha=50$ and $\chi=0.889$, the slurry formed an interesting front. In Figure 23, you can see it close-up of the first run. This interesting ridge was seen in all four runs of the same experiment. This may have occurred because more of the fluid was inclined to move towards the fingers since the fingers moved faster than the hinges between them. Furthermore, if the front of the fluid ridge stopped the excess fluid on top from surpassing it, a small ridge of its own could have been formed. However, more experimentation and analysis needs to be done to explain such an affect.

5.3 Height Profile

While we were able to observe the different regimes, we did not have a way of quantifying the difference in heights of the fluids until we implemented the height tracking code. The implementation of this code in our analysis coincided with the time we started doing our constant flux experiments.

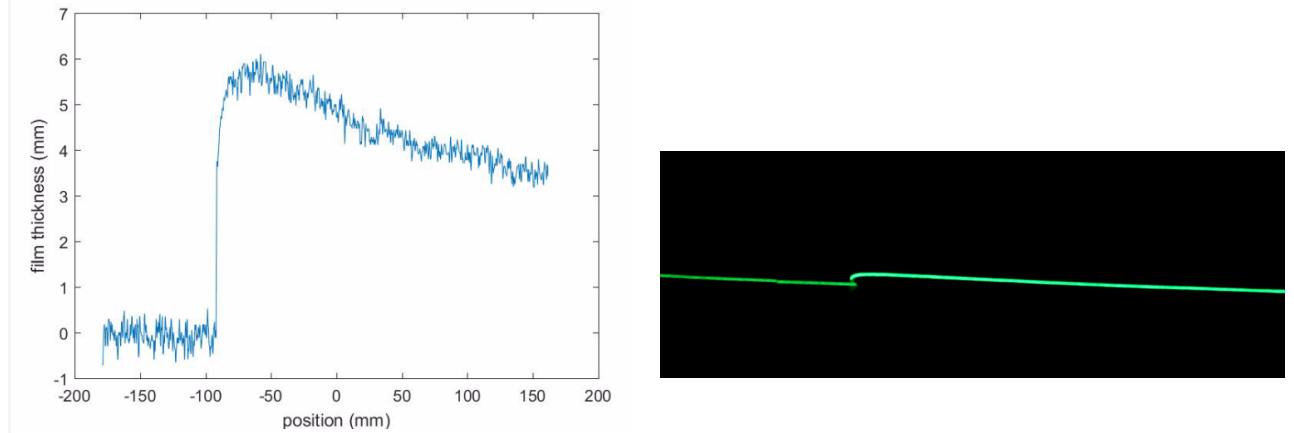


Figure 24: Height profile for $\alpha = 50$ and $\chi = 0.389$ as captured by our code.

Figure 25: Height profile for $\alpha = 50$ and $\chi = 0.389$ as captured by our camera.

Figure 24 shows the graph generated by the height profile code that corresponds to Figure 25 (a frame taken from a height tracking video in which the fluid flows from the right side of the frame to the left). The point in which there is a spike in the graph from 0 mm to about 6 mm corresponds to the front of the fluid. As indicated in Figure 19, we expect an experiment with $\alpha = 50$ and $\phi = 0.45$ to display a ridged regime. The graph confirms that this was the ridged regime because the front part of the fluid is raised about 3 mm higher than fluid farther right in the image.

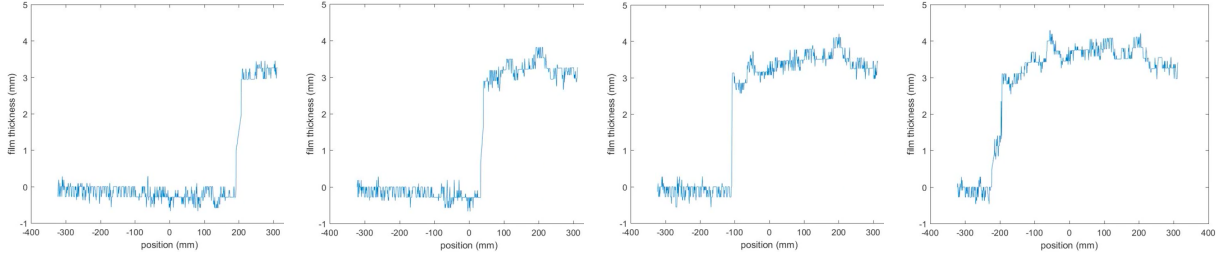


Figure 26: From left to right, four screen shots of the height profile at $\alpha = 20$ and $\chi = 0.88$ taken 32 seconds apart.

Figure 26 is created from the analysis of an experiment with $\alpha = 20$ and $\phi = 0.25$. We observed the separation of particles during the experiment, which agrees with our expectation of a settled regime because of the low angle and concentration. Furthermore with the height tracking code we were able to see a difference between these graphs and those generated from the ridged regime experiment. While the ridged regime graphs show a raised front, the graphs for the settled regime show a relatively constant height throughout the whole fluid. There is a slightly raised region in the middle of the fluid which may correspond to the area with a higher concentration of particles when settled. The height of the whole settled fluid is about 3-4mm which is lower than the ridge but interestingly is about the same as the back part of the fluid in the ridged regime.

6 Experimental Error

Experimental error could be caused by the equipment we used. The scale used to measure the mass of PDMS and particles is accurate up to a tenth of a gram and the measurement fluctuates by 0.1 grams. To prepare a mixture of PDMS and particles, we used a spatula to mix the substance and therefore, some of our substance was left in it. When pouring the mixture of PDMS and particles in the track, not all of the mixture will be poured into the track due to the residual left in the container, which may change the density of the substance traveling down the track. Another cause for experimental error is that containers from previous experiments were used, which means that we could have obtained a small amount of particles from previous experiments left in container.

7 Conclusion

A particle laden flow is a mixture of fluid and particles with no chemical reactions. This series of experiments consisted of bidensity particle laden flows down a straight incline with an adjustable angle. Previous studies have been done in the lab with a monodisperse mixture of PDMS. Like mentioned throughout the report, particle laden flows can be separated into three regimes: ridged regime, settled regime, and a well-mixed regime. The three regimes result from varying particle concentration and the

angle of the track. In a ridged regime, the shear induced migration (z-direction) is dominant over gravitational force causing particles to be pushed up in the z-direction, as the slurry travels down the track. The dominant shear forces cause particles to be suspended in the fluid rather than sink, which results in a higher concentration of particles at the fluid front. Higher particle concentration causes the fluid front to be thicker. Ridged regime results from higher concentrations of particles and/or a steeply angled track. Settled regime results when gravitational forces are dominant over shearing forces; this causes particles to sink in the downward direction toward the surface of the track. A settled regime results from lower concentrations of particles and/or a less steep incline. In addition to the settled and ridged regimes, there is a well-mixed regime, which can occur when the separation between the particles and PDMS is not observed.

Two methods of flow were studied: constant volume of fluid and constant flux. We hypothesized the front position to behave similar to $t^{1/3}$. Results obtained showed that the front position behaves as predicted, with minor discrepancies. After performing data analysis, it was confirmed that the slurry behaves more closely to its theoretical values towards the end of the run when more time has passed. Front tracking results of monodisperse were similar to those found from bidisperse experiments. Therefore, it is believed that both monodisperse and bidisperse behave similarly.

Further studies could be made to monitor the fingering with respect to angle of incline and particle density. Low particle concentration flow on a low inclined track tends to result in multiple fingers forming. While high concentration flow on a high inclined track tends to result in minimal fingering and rather just one thick finger. This phenomenon may possibly be explained from mixture viscosity, which causes particles to stick together and not create multiple fingers. A good future study could include changing variables for instance angle of incline or other particles densities. Additionally, a longer track would allow us to obtain closer results that correlate with theory. Due to the many interesting behaviors of slurries many questions can be explored for further research.

8 Acknowledgements

The 2017 UCLA particle slurry team would like to thank Professor Andrea Bertozzi and the team's mentors, Professor Michael Lindstrom, Professor Claudia Falcon, and Professor David Arnold for their advice and help. We acknowledge financial support from the NSF grant DMS-1312543.

References

- [1] Frans De Rooij. *Sedimenting particle-laden flows in confined geometries*. PhD thesis, University of Cambridge, 2000.
- [2] Sungyon Lee, Jeffrey Wong, and Andrea L Bertozzi. Equilibrium theory of bidensity particle-laden flows on an incline. In *Mathematical Modelling and Numerical Simulation of Oil Pollution Problems*, pages 85–97. Springer, 2015.
- [3] Yu Liu and Joo-Hwa Tay. The essential role of hydrodynamic shear force in the formation of biofilm and granular sludge. *Water research*, 36(7):1653–1665, 2002.
- [4] Sungyon Lee, Yvonne Stokes, and Andrea L Bertozzi. Behavior of a particle-laden flow in a spiral channel. *Physics of Fluids*, 26(4):1661–1673, 2014.
- [5] Benjamin P Cook, Andrea L Bertozzi, and AE Hosoi. Shock solutions for particle-laden thin films. *SIAM Journal on Applied Mathematics*, 68(3):760–783, 2008.
- [6] Thomas Ward, Chi Wey, Robert Glidden, AE Hosoi, and AL Bertozzi. Experimental study of gravitation effects in the flow of a particle-laden thin film on an inclined plane. *Physics of Fluids*, 21(8):083305, 2009.
- [7] N Murisic, J Ho, V Hu, P Latterman, T Koch, K Lin, M Mata, and AL Bertozzi. Particle-laden viscous thin-film flows on an incline: Experiments compared with a theory based on shear-induced migration and particle settling. *Physica D: Nonlinear Phenomena*, 240(20):1661–1673, 2011.
- [8] Jeffrey T Wong and Andrea L Bertozzi. A conservation law model for bidensity suspensions on an incline. *Physica D: Nonlinear Phenomena*, 330(1):47–57, 2016.
- [9] Sungyon Lee, Aliki Mavromoustaki, Gilberto Urdaneta, Kaiwen Huang, and Andrea L Bertozzi. Experimental investigation of bidensity slurries on an incline. *Granular Matter*, 16(2):269–274, 2014.
- [10] Irvin M Krieger and Thomas J Dougherty. A mechanism for non-newtonian flow in suspensions of rigid spheres. *Journal of Rheology*, 3(1):137–152, 1959.
- [11] U Schaflinger, A Acrivos, and K Zhang. Viscous resuspension of a sediment within a laminar and stratified flow. *International Journal of Multiphase Flow*, 16(4):567–578, 1990.
- [12] Ronald J Phillips, Robert C Armstrong, Robert A Brown, Alan L Graham, and James R Abbott. A constitutive equation for concentrated suspensions that accounts for shear-induced particle migration. *Physics of Fluids A: Fluid Dynamics*, 4(1):30–40, 1992.
- [13] N Murisic, B Pausader, D Peschka, and AL Bertozzi. Dynamics of particle settling and resuspension in viscous liquid films. *Journal of Fluid Mechanics*, 717(1):203–231, 2013.
- [14] L Wang, A Mavromoustaki, AL Bertozzi, G Urdaneta, and K Huang. Rarefaction-singular shock dynamics for conserved volume gravity driven particle-laden thin film. *Physics of Fluids*, 27(3):033301, 2015.
- [15] Patrick Flynn, Joseph Pappe, Aviva Prins, William Sisson, Samuel Stanton, and Ruiyi Yang. Constant flux particle-laden viscous thin film flows on an incline, aug 2016.